(Received 4 June 2025, Accepted 8 August 2025, Scheduled 19 August 2025)

A Multiband Planar Antenna with Asymmetric CPW Feeding for WLAN, UAV Communications, and 5G

Wei Ding[1], Ziyi Su[1], and Weina Liu[2,*]

[1] College of Mechanical Engineering, Jiangsu University of Technology, Changzhou 213001, Jiangsu, China
[2] College of Telecommunication and Information Engineering
Jiangsu University of Technology, Changzhou 213001, Jiangsu, China

ABSTRACT: A multiband planar antenna fed by an asymmetric coplanar waveguide (ACPW) is proposed and fabricated. The design incorporates branched stubs within split-ring resonator (SRR) and integrates this modified SRR with the ACPW structure, thereby expanding the antenna's operational bandwidth and improving gain performance. The antenna has dimensions of 60 mm × 58 mm × 0.813 mm, which are equivalent to $0.48\lambda_0 \times 0.46\lambda_0 \times 0.0065\lambda_0$ at 2.4 GHz. Simulation and measurement results demonstrate close agreement. The antenna exhibits $|S_{11}| < -10$ dB in the frequency bands of 2.23–2.51 GHz, 3.54–4.47 GHz, and 5.01–6.29 GHz, with a maximum gain of 7.07 dBi at 5.1 GHz and over 2.5 dBi gain across all bands. This antenna meets the requirements for WLAN, UAV communications, and 5G applications.

1. INTRODUCTION

In recent years, remarkable breakthroughs have been made in the fields of fifth-generation (5G) mobile communications, drones, and wireless local area networks (WLANs). Consequently, the demand for high-performance antennas for modern wireless communication systems has shown exponential growth.

In complex electromagnetic environment engineering scenarios, the combination of wide-band coverage characteristics (e.g., compatibility with 2.4/5.8 GHz dual bands) and high gain performance has become an important technical index for the development of wireless communication equipment.

In this context, planar antennas have become a crucial research focus for radio frequency (RF) front-end integrated design. Their key advantages, such as compact size, low profile, and compatibility with standard manufacturing processes, make them highly attractive. In particular, coplanar waveguide (CPW)-fed planar antennas with asymmetric topology optimization can break through the limitations of traditional symmetric structures. This approach enables significant improvements in both operational bandwidth and radiation efficiency. These benefits highlight the importance and necessity of further exploring ACPW-fed multiband planar antennas.

In recent years, multi-band antenna design has seen the introduction of various innovative structures, such as defective ground structure [1–6], inverted-L structure [7–9], parasitic structure [10–13], and slotting technique on radiating surfaces [14]. Defective ground structure modifies surface current distribution via geometric cuts or etches on the ground plane, enabling multi-band operation. Inverted-L structure excites electromagnetic radiation at distinct frequencies through its unique spatial layout, while parasitic structure expands the operational frequency range via electromagnetic coupling with the main radiator. Meanwhile, slotting technique achieves multi-band radiation by precisely controlling current paths through adjustments to slot geometry, dimensions, and positioning. These approaches significantly enhance antenna performance and drive advancements in multi-band technology.

Notably, metamaterials have shown remarkable potential in antenna design. Their unusual electromagnetic properties enable flexible field distribution regulation, offering a novel approach to multi-band design. Among them, loading techniques based on split-ring resonators (SRRs) and their derivatives have become a research focus. For example, SRR loading structures [15–17] and square SRR structures [18–21] trigger resonance effects to excite additional radiation bands. Etching SRR or complementary split-ring resonator (CSRR) on radiating surfaces [22–27] or ground planes [28–30] further enhances multi-frequency performance by optimizing electromagnetic coupling with the antenna body.

Although existing antennas reported in the literature have been optimized to achieve multi-band communication requirements through different structures, the existing designs generally face the challenge of maintaining good radiation gain during multi-band operation.

This paper introduces an ACPW-fed tri-band planar antenna with overall dimensions of 60 mm × 58 mm × 0.813 mm. The bandwidth and gain performance of the antenna are improved by adding branches inside an SRR structure. Additionally, the integration of the SRR structure with an ACPW structure also contributes to the performance improvement. Furthermore, measurement results show that the antenna has a return loss of less than −10 dB in the 2.23–2.51 GHz, 3.54–4.47 GHz, and 5.01–6.29 GHz bands, and achieves a relatively high ra-

* Corresponding author: Weina Liu (naliu529_i5@163.com).

TABLE 1. Antenna geometry.

parameters	dimensions/mm	parameters	dimensions/mm	parameters	dimensions/mm
L_0	58	b	2.5	$L_1 = c$	1
W_0	60	q	0.23	L_2	1.8
$S = e$	6	W_f	3.94	L_3	11
u	20	L_f	10	L_4	8
N	3.5	R_1	16	L_5	4.4
p	18	R_2	15	L_6	3.6
M	12	k	24.8	L_7	3

diation gain, with the maximum gain reaching 7.07 dBi. The proposed antenna meets the band requirements of WLAN, unmanned aerial system (UAS), and certain frequency ranges of 5G.

2. ANTENNA DESIGN AND ANALYSIS

The antenna structure proposed in this paper is shown in Fig. 1. Specifically, the antenna is printed on a 0.813 mm thick ROC4003c substrate with a relative dielectric constant of 3.38 and a loss angle tangent of 0.0027 as shown in Table 1.

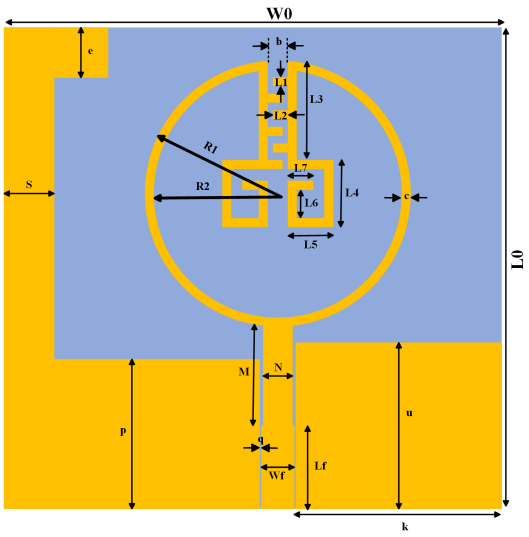

FIGURE 1. Antenna structure schematic.

The antenna proposed in this paper adopts an ACPW feeding scheme. The asymmetric structure of the ACPW provides more independently adjustable parameters, thereby offering greater design flexibility and superior impedance matching. The signal line width Wf is 3.94 mm, and the gap q between the two sides of the signal line is 0.23 mm, which enables impedance matching to a characteristic impedance of 50 ohms.

In antenna design, the resonant frequency (f) and input impedance (z_{in}) are two core parameters that jointly determine the antenna's radiation efficiency and impedance matching performance. The resonant frequency of the antenna is determined by the interaction between the internal equivalent inductance (L) and capacitance (C), as expressed in Equation (1). This equation describes how the values of inductance and capacitance interact to define the specific frequency at which the antenna will resonate.

$$f_0 = \frac{1}{2\pi\sqrt{LC}} \tag{1}$$

When the operating frequency equals the resonant frequency (f_0), the antenna operates in resonance. At this frequency, the imaginary part (x_{in}) of the input impedance approaches zero, and the impedance characteristic is reduced to a purely resistive form, as expressed in Equation (2). This relationship is crucial for ensuring optimal impedance matching, which in turn affects the overall performance of the antenna.

$$z_{in} = \frac{U_{in}}{I_{in}} = R_{in} + jX_{in} \overset{Resonance}{\rightarrow} z_{in} \approx R_{in} \tag{2}$$

The simplified equivalent circuit of the antenna is shown in Figure 2.

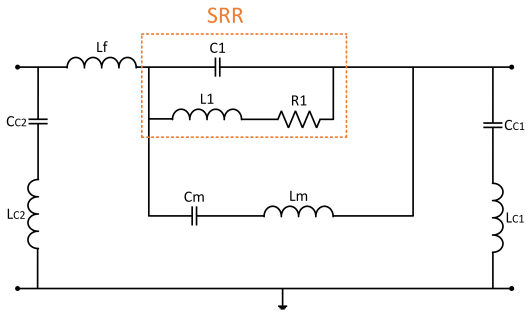

FIGURE 2. Simplified equivalent circuit diagram of the antenna.

Figures 3(a)–(d) depict the 4-stage design process involved in the proposed antenna design. Fig. 4 illustrates the simulated input reflection coefficient (S_{11}) results for the 4 design stages (Stage 1 to Stage 4). Fig. 3(a) shows the symmetric CPW-fed SRR patch antenna, which has a resonant frequency of 6.7 GHz as shown in Fig. 4 (stage 1). Fig. 3(b) presents an SRR patch antenna with symmetric CPW feeding, which is formed by adding bilateral ground planes. As reflected in the circuit model of Fig. 2, this structural modification is manifested by an increase in the values of Lc_1 and Lc_2. Corresponding to Stage 2 in Fig. 4, the resonant frequency of this antenna is 6.4 GHz. For Fig. 3(c), extending the left ground plane further tunes the resonant frequency to 6.3 GHz, a modification that increases the value of Lc_2 in the circuit model of Fig. 2. This structure is

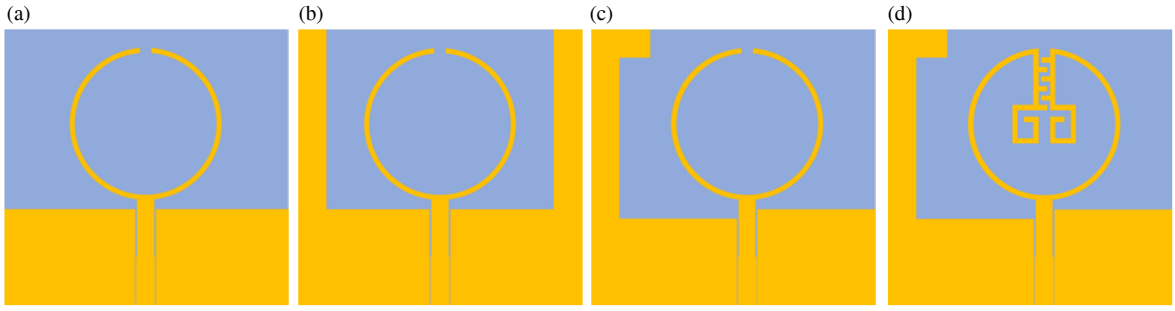

FIGURE 3. Design stages of proposed antenna.

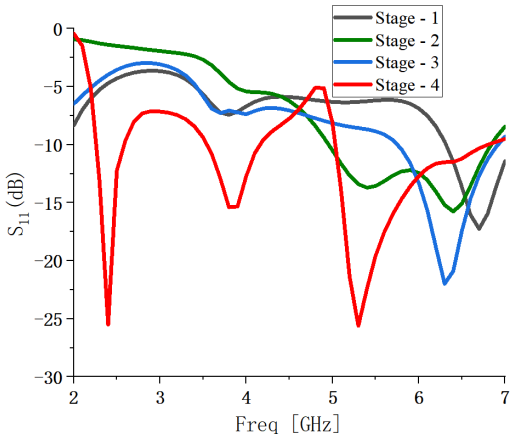

FIGURE 4. Comparison of S_{11} at different design stages.

formed with asymmetric grounding and an ACPW feed. Meanwhile, as illustrated in Fig. 4, the S_{11} of Stage 3 at the resonant frequency is 7 dB lower than that of Stage 2, indicating that the impedance matching performance of Stage 3 is superior to that of Stage 2. Finally, Fig. 3(d) shows that by incorporating branches of different lengths into the SRR, the corresponding circuit model in Fig. 2 is represented as the SRR being in series with C_m and L_m. These two components modify the reactance characteristics of the resonant circuit and, in conjunction with the design of Stage 4 in Fig. 4, ultimately enable the antenna to form three resonant points at 2.4 GHz, 3.8 GHz, and 5.3 GHz.

3. SIMULATION RESULTS AND ANALYSIS

Figures 5(a)–(c) illustrate the simulated current surface distribution of the proposed antenna at three resonant frequencies. From Fig. 5, it can be seen that the antenna feedline current is large at these three resonant frequencies, indicating that the antenna is in operation and has good impedance matching. Specifically, the current distribution of the antenna at 2.4 GHz mainly originates from the SRR and the left ground plane, while at 3.8 GHz and 5.3 GHz, it mainly originates from the SRR and its internal branches.

To confirm the resonance mechanism of the antenna and investigate the relationship between the antenna resonance and antenna parameters, a study was carried out by varying dimensions of the SRR and its internal branches as shown in Figs. 6(a)–(d). Fig. 6(a) demonstrates the effect of parametric tuning of the outer diameter R_1 of the SRR from 16 mm to 16.8 mm on the resonance characteristics. It is observed that as the value of R_1 increases, both the second and third resonant frequency points shift towards lower frequencies, while the first resonant frequency point does not show any significant displacement. When $R_1 = 16$ mm, the antenna presents the best impedance matching characteristic at the first resonance point, while this characteristic shows a significant decreasing trend with the increase of R_1. Fig. 6(b) demonstrates the effect of parametric tuning on the resonance characteristics over the SRR ring width c from 0.2 mm to 1 mm. It is observed that the impedance matching at the first resonant frequency point is significantly improved with increasing values of c, and better matching is obtained for $c = 1$ mm. Thus, it can be easily demonstrated that the first resonance is caused by the SRR structure. Fig. 6(c) demonstrates the effect of parametric tuning of branch L_4 from 8 mm to 10 mm on the resonant characteristics. It is observed that increasing the value of L_4 significantly decreases the impedance matching at the third resonant frequency point, and better impedance matching is obtained when $L_4 = 8$ mm. In addition to the effect of branch L_4, the influence of branch L_6 on the resonant characteristics is also investigated. Fig. 6(d) shows the effect of parametric tuning of branch L_6 from 3.4 mm to 5.8 mm on the resonant characteristics. It is observed that the third resonant frequency disappears at $L_6 = 3.4$ mm; the second resonant frequency disappears at $L_6 = 5.8$ mm; and both the second and third resonant frequencies show optimal impedance matching at $L_6 = 4.6$ mm. Thus, it can be easily demonstrated that the second and third resonances are due to the branching inside the SRR.

In light of the aforementioned conclusion, the final optimized antenna was physically manufactured, and a photograph of the proposed antenna was presented in Fig. 7. Subsequently, measurements were carried out using a vector network analyser as depicted in Fig. 8. The three operating bands of the antenna have bandwidths of 280 MHz (2.23–2.51 GHz, relative bandwidth 11.8%), 930 MHz (3.54–4.47 GHz, relative bandwidth 23.2%), and 1280 MHz (5.01–6.29 GHz, relative bandwidth 22.8%). These bands meet the band requirements for WLAN, unmanned aerial vehicle (UAV), and 5G. Fig. 9 illustrates the comparison of the simulated and measured S_{11}, and it is evident that the measured impedance matching outperforms the simulated results.

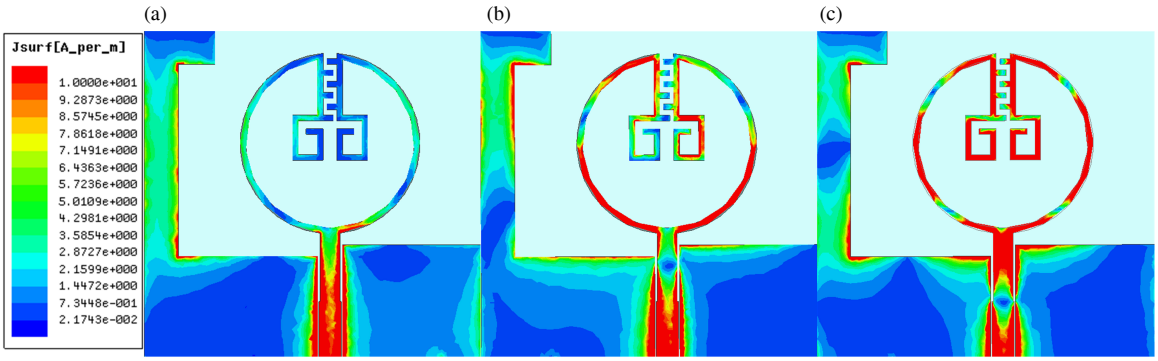

FIGURE 5. Current distribution of proposed antenna. (a) 2.4 GHz. (b) 3.8 GHz. (c) 5.3 GHz.

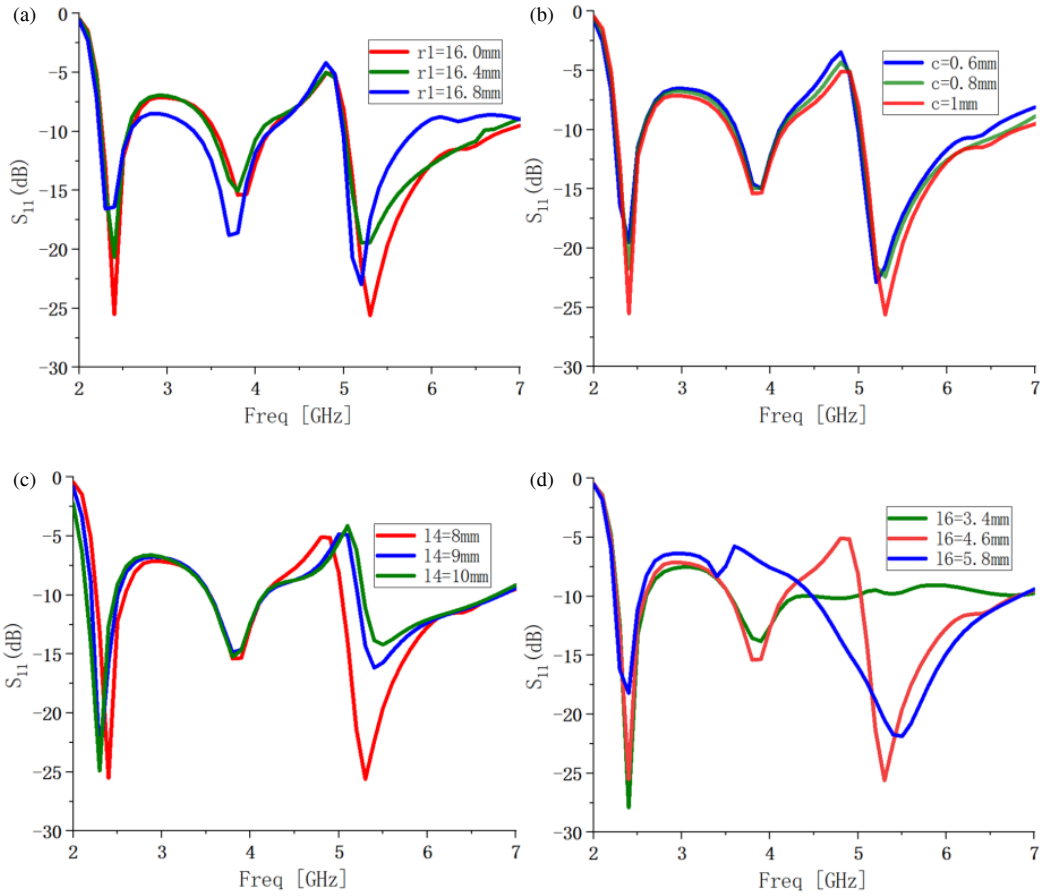

FIGURE 6. Influence of key structural parameters (r_1, c, l_4, l_6) on S_{11}.

Figure 10 presents a comparison between the simulated and measured results of the far-field radiation patterns in the E-plane and H-plane at the frequencies of 2.4 GHz, 3.8 GHz, and 5.3 GHz. Fig. 11 shows the 3D gain pattern of the antenna at 2.4 GHz, 5.2 GHz, and 5.8 GHz, and the antenna has a gain of 3.4 dBi, 7 dBi, and 6 dBi respectively at these frequencies, which can be used in a practical communication system. Fig. 12 shows the simulated maximum gain of the antenna from 2.23 GHz to 6.29 GHz. The antenna has lower gain at lower frequencies because there are fewer current distribution paths. As the frequency increases, the number of current distribution paths increases, and the gain increases gradually.

4. ANTENNA PERFORMANCE COMPARISON

From Table 2, it can be seen that the present antenna achieves a maximum gain of 4.11 dBi in the 2.23–2.51 GHz band, a maximum gain of 6.51 dBi in the 3.54–4.47 GHz band, and a maximum gain of 7.07 dBi in the 5.01–6.29 GHz band.

The overall size of the antenna designed in this study is 60 mm × 58 mm × 0.813 mm, which is both lightweight and compact. The antenna covers multiple frequency bands required for UAV communication with gains of 3.44 dBi at 2.4 GHz, 6.9 dBi at 5.2 GHz, and 5.98 dBi at 5.8 GHz, respectively. Moreover, its compact size, lightweight structure,

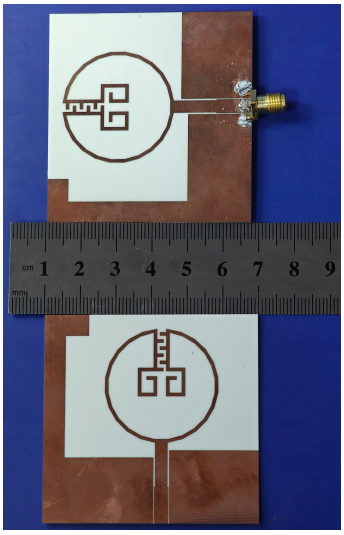

FIGURE 7. Photograph of the proposed antenna.

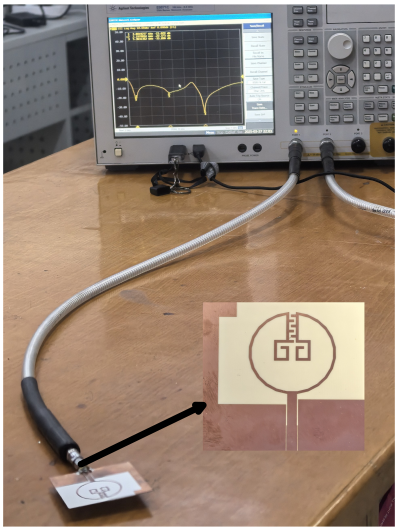

FIGURE 8. Measurement of proposed antenna S_{11} with a vector network analyzer.

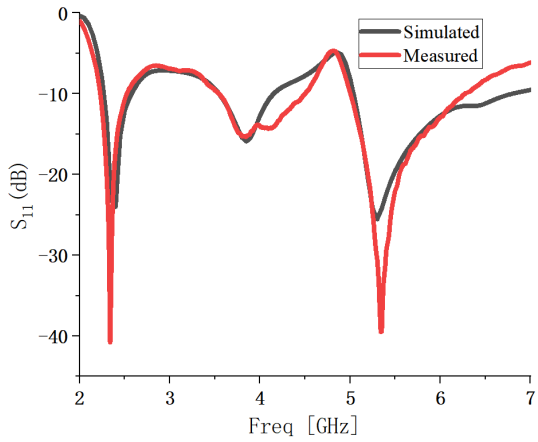

FIGURE 9. Comparison between simulated and measured S_{11} of the proposed antenna.

and high gain in multiple frequency bands make the antenna ideal for UAV communication scenarios, and it also meets the antenna performance requirements of WLAN and 5G.

In comparison, small-sized designs (such as those in [20] and [25]) are compact but exhibit significant gain fluctuations when covering multiple frequency bands. For instance, the antenna in [20] has a gain ranging from 1.66 dBi to 3.87 dBi within 2.23–5.90 GHz band. The antenna in [5] also suffers from low gain, with its performance in corresponding frequency bands being notably below expectations. In contrast, our $60 \times 58\,\text{mm}^2$ design achieves more stable and gradually increasing gain (4.11–7.07 dBi) across three frequency bands within 2.23–6.29 GHz.

When comparing performance in the same frequency bands (e.g., 2.23–2.51 GHz), the gain values reported in literature are 3.3 dBi in [1], 1.94 dBi in [20], and the gain of the antenna in [5] is also at a low level, while our design reaches 4.11 dBi. In the high-frequency band (5.01–6.29 GHz), our design achieves a gain of 7.07 dBi, which is superior to 5.41 dBi of the design in [30] within the same band. These results fully demonstrate the advantages of our design in terms of gain performance.

TABLE 2. Comparison of the proposed antenna with the existing antenna.

References	dimensions/mm	frequency/GHz	Peak Gain/dBi
[1]	40×40	2.24–2.93	3.3
		4.48–5.54	5.7
[5]	50×30	1.42–2.08	2.10
		3.49–4.13	1.75
		5.23–7.53	2.50
[20]	35×34	2.23–2.51	1.94
		2.98–3.11	2.2
		3.42–3.57	1.66
		4.82–5.15	3.87
		5.71–5.90	3.65
[25]	32×38	2.4–2.6	3.8
		2.9–3.1	3.2
		3.3–3.5	1.8
		4.0–8.3	5.1
[30]	60×60	2.45	1.03
		3.56	5.10
		5.60	5.41
This work	60×58	2.23–2.51	4.11
		3.54–4.47	6.51
		5.01–6.29	7.07

Of course, we are clearly aware of certain limitations in our design. In terms of size, the $60 \times 58\,\text{mm}^2$ specification has obvious shortcomings in miniaturization compared with some small-sized schemes in the literature, which may restrict its application in scenarios with extremely strict space constraints.

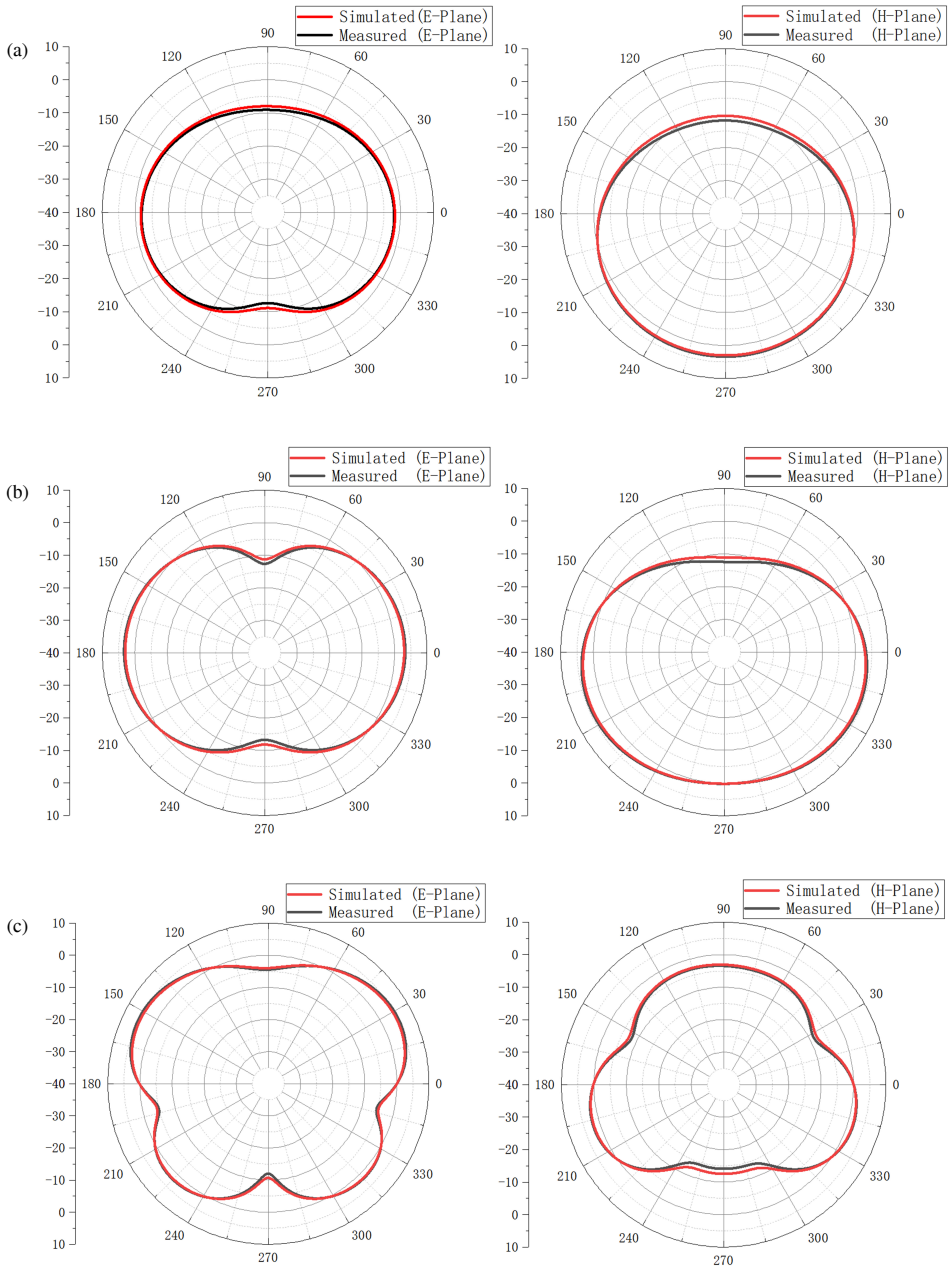

FIGURE 10. Far-field radiation pattern. (a) 2.4 GHz. (b) 3.8 GHz. (c) 5.3 GHz.

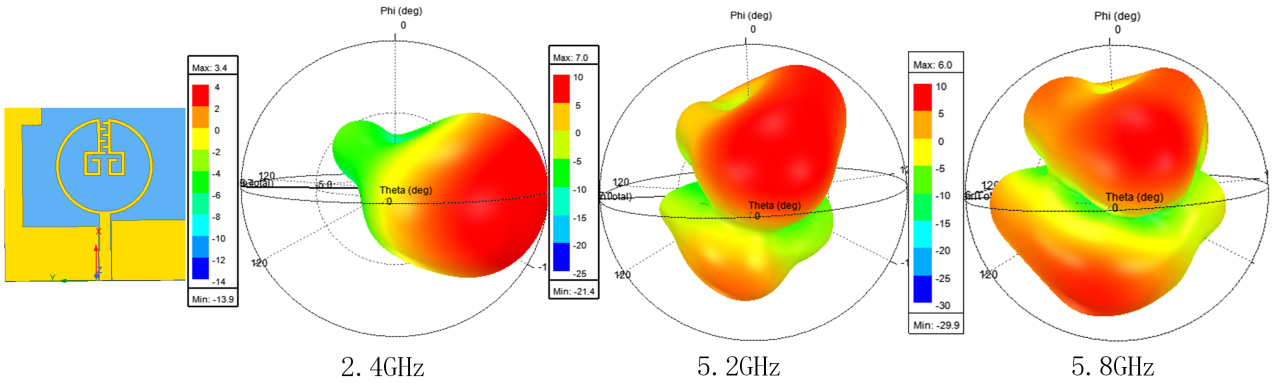

FIGURE 11. 3D gain pattern.

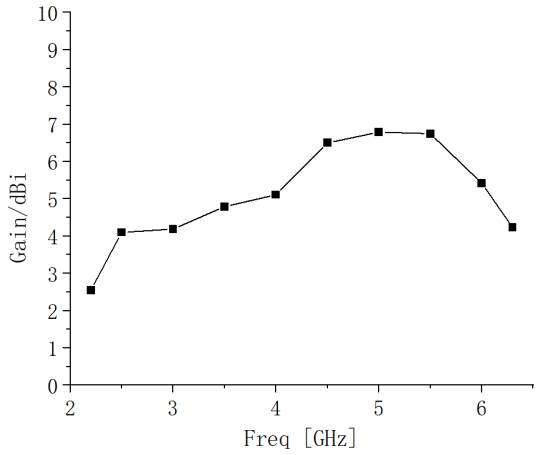

FIGURE 12. Simulated maximum gain of the proposed antenna.

In the future, while ensuring the existing gain performance, we will actively draw on ideas and experiences in miniaturization design from relevant literature, exploring ways to further reduce the antenna size by adopting new substrate materials and optimizing the layout of the radiation structure, with the aim of expanding its practical application scope.

5. CONCLUSION

In this study, a multi-band planar antenna based on ACPW feed and SRR structure is successfully designed and fabricated. By innovatively introducing a branch structure inside the SRR unit and combining the branch structure with an ACPW feed system, we optimize the antenna's multiband characteristics and radiation performance by balancing their mutual influences and design trade-offs. The test results show that the antenna exhibits good impedance matching characteristics in the three frequency bands of 2.23–2.51 GHz, 3.54–4.47 GHz, and 5.01–6.29 GHz, and achieves a peak gain of 7 dBi at 5.1 GHz. Moreover, in all the operating frequency bands, the high degree of agreement between simulated and measured data verifies the effectiveness of the design method. The obtained wide-band coverage successfully meets the technical requirements of modern wireless communication systems, such as WLAN, UAV communication, and 5G communication.

ACKNOWLEDGEMENT

This work was supported by the Natural Science Foundation of Changzhou under Grant CJ20230035.

REFERENCES

[1] Yassen, M. T., M. R. Hussan, H. A. Hammas, H. Al-Saedi, and J. K. Ali, "A dual-band printed antenna design based on annular Koch snowflake slot structure," *Wireless Personal Communications*, Vol. 104, No. 2, 649–662, 2019.

[2] Zhang, L., J. Su, and X. Chen, "A single-feed tri-band conformal circularly polarized dual-annular slot antenna," in *2019 Cross Strait Quad-Regional Radio Science and Wireless Technology Conference (CSQRWC)*, 1–3, Taiyuan, China, 2019.

[3] Karthikeyan, M., R. Sitharthan, T. Ali, S. Pathan, J. Anguera, and D. S. Sundar, "Stacked T-shaped strips compact antenna for WLAN and WiMAX applications," *Wireless Personal Communications*, Vol. 123, No. 2, 1523–1536, 2022.

[4] Gyasi, K. O., G. Wen, D. Inserra, Y. Huang, E. A. Ampoma, J. Li, M. A. Basit, and H. B. Zhang, "Tri-band planar monopole antenna with two circularly polarised bandwidths for WiMAX applications," *IET Microwaves, Antennas & Propagation*, Vol. 12, No. 15, 2350–2355, 2018.

[5] Nadh, B. P., B. T. P. Madhav, and M. S. Kumar, "Design and analysis of dual band implantable DGS antenna for medical applications," *Sādhanā*, Vol. 44, No. 6, 131, 2019.

[6] Chang, T.-N. and J.-M. Lin, "Dual-band circularly polarized monopole antenna," *Journal of Electromagnetic Waves and Applications*, Vol. 29, No. 7, 843–857, 2015.

[7] Bag, B., P. Biswas, S. De, S. Biswas, and P. P. Sarkar, "A wide multi-band monopole antenna for GSM/WiMAX/WLAN/X-band/Ku-band applications," *Wireless Personal Communications*, Vol. 111, No. 1, 411–427, 2020.

[8] Lu, J.-H., B.-R. Zeng, and Y.-H. Li, "Planar multi-band monopole antenna for WLAN/WiMAX applications," in *2014 International Symposium on Antennas and Propagation Conference Proceedings*, 475–476, Kaohsiung, Taiwan, 2014.

[9] Midya, M., S. Bhattacharjee, and M. Mitra, "CPW-fed dual-band dual-sense circularly polarized antenna for WiMAX application," *Progress In Electromagnetics Research Letters*, Vol. 81, 113–120, 2019.

[10] Alam, M. M., R. Azim, N. M. Sobahi, A. I. Khan, and M. T. Islam, "A dual-band CPW-fed miniature planar antenna for S-, C-, WiMAX, WLAN, UWB, and X-band applications," *Scientific Reports*, Vol. 12, No. 1, 7584, 2022.

[11] Shakib, M. N., M. Moghavvemi, and W. N. L. B. W. Mahadi, "Design of a tri-band off-body antenna for WBAN communication," *IEEE Antennas and Wireless Propagation Letters*, Vol. 16, 210–213, 2016.

[12] Liu, F., K. Xu, P. Zhao, L. Dong, and G. Wang, "Uniplanar dual-band printed compound loop antenna for WLAN/WiMAX applications," *Electronics Letters*, Vol. 53, No. 16, 1083–1084, 2017.

[13] Hajlaoui, E. A., "New triple band electromagnetic band gap microstrip patch antenna with two shaped parasitic elements," *Journal of Computational Electronics*, Vol. 17, No. 1, 452–457, 2018.

[14] Zhai, H., L. Liu, Z. Ma, and C. Liang, "A printed monopole antenna for triple-band WLAN/WiMAX applications," *International Journal of Antennas and Propagation*, Vol. 2015, No. 1, 254268, 2015.

[15] Ameen, M., A. Mishra, and R. K. Chaudhary, "Asymmetric CPW-fed electrically small metamaterial-inspired wideband antenna for 3.3/3.5/5.5 GHz WiMAX and 5.2/5.8 GHz WLAN applications," *AEU — International Journal of Electronics and Communications*, Vol. 119, 153177, 2020.

[16] Kukreja, J., D. K. Choudhary, and R. K. Chaudhary, "CPW fed miniaturized dual-band short-ended metamaterial antenna using modified split-ring resonator for wireless application," *International Journal of RF and Microwave Computer-Aided Engineering*, Vol. 27, No. 8, e21123, 2017.

[17] Ali, T., M. M. Khaleeq, S. Pathan, and R. C. Biradar, "A multiband antenna loaded with metamaterial and slots for GPS/WLAN/WiMAX applications," *Microwave and Optical Technology Letters*, Vol. 60, No. 1, 79–85, 2018.

[18] Pandey, S. K., *et al.*, "Printed CPW-fed dual-band antenna using square closed-ring and square split-ring resonator," *Applied Physics A*, Vol. 126, No. 8, 626, 2020.

[19] Saraswat, R. K. and M. Kumar, "Implementation of hybrid fractal metamaterial inspired frequency band reconfigurable multiband antenna for wireless applications," *International Journal of RF and Microwave Computer-Aided Engineering*, Vol. 30, No. 9, e22315, 2020.

[20] Saraswat, R. K. and M. Kumar, "A metamaterial hepta-band antenna for wireless applications with specific absorption rate reduction," *International Journal of RF and Microwave Computer-Aided Engineering*, Vol. 29, No. 10, e21824, 2019.

[21] Ali, T. and R. C. Biradar, "A compact multiband antenna using λ/4 rectangular stub loaded with metamaterial for IEEE 802.11N and IEEE 802.16E," *Microwave and Optical Technology Letters*, Vol. 59, No. 5, 1000–1006, 2017.

[22] Chaurasia, P., B. K. Kanaujia, S. Dwari, and M. K. Khandelwal, "Design and analysis of seven-bands-slot-antenna with small frequency ratio for different wireless applications," *AEU — International Journal of Electronics and Communications*, Vol. 99, 100–109, 2019.

[23] Boopathi Rani, R. and S. K. Pandey, "A CPW-fed circular patch antenna inspired by reduced ground plane and CSRR slot for UWB applications with notch band," *Microwave and Optical Technology Letters*, Vol. 59, No. 4, 745–749, 2017.

[24] Sharma, S. K. and R. K. Chaudhary, "Dual-band metamaterial-inspired antenna for mobile applications," *Microwave and Optical Technology Letters*, Vol. 57, No. 6, 1444–1447, 2015.

[25] Rao, M. V., B. T. P. Madhav, T. Anilkumar, and B. P. Nadh, "Metamaterial inspired quad band circularly polarized antenna for WLAN/ISM/Bluetooth/WiMAX and satellite communication applications," *AEU — International Journal of Electronics and Communications*, Vol. 97, 229–241, 2018.

[26] Daniel, R. S., R. Pandeeswari, and S. Raghavan, "A compact metamaterial loaded monopole antenna with offset-fed microstrip line for wireless applications," *AEU — International Journal of Electronics and Communications*, Vol. 83, 88–94, 2018.

[27] Bhattacharjee, S., S. Maity, S. R. B. Chaudhuri, and M. Mitra, "Metamaterial-inspired wideband biocompatible antenna for implantable applications," *IET Microwaves, Antennas & Propagation*, Vol. 12, No. 11, 1799–1805, 2018.

[28] Yao, H., X. Liu, H. Zhu, H. Li, G. Dong, and K. Bi, "Dual-band microstrip antenna based on polarization conversion metasurface structure," *Frontiers in Physics*, Vol. 8, 279, 2020.

[29] Rosaline, S. I. and S. Raghavan, "CSRR-based compact penta band printed antenna for GPS/GSM/WLAN/WiMAX applications," *Microwave and Optical Technology Letters*, Vol. 57, No. 7, 1538–1542, 2015.

[30] Ali, W., E. Hamad, M. Bassiuny, and M. Hamdallah, "Complementary split ring resonator based triple band microstrip antenna for WLAN/WiMAX applications," *Radioengineering*, Vol. 26, No. 1, 78–84, 2017.